Effect of a Buried-Wire Gage on the Separation Bubble—Numerical Study

David Degani*
NASA Ames Research Center, Moffett Field, California

A numerically simulated buried-wire separation gage is investigated with emphasis on its effect on the separation bubble. The conjugated problem of a supersonic, time-dependent, two-dimensional flowfield above a conductive solid wall with an embedded heat source is solved using implicit finite difference algorithms. Steady-state and transient cases were computed for different locations of the heat source within the bubble. Results show that by using a steady heat source, the flow direction near the wall can be detected, without distorting the flowfield, only if the source is located in regions where the bubble is thick (i.e., not too close to the separation). The flow direction near separation can be detected by using a temperature pulse at the solid/fluid interface with insignificant distortion of the flowfield.

Introduction

THE hot-wire surface gage for boundary-layer separation detection has been employed successfully in recent years.[1-3] Unlike the alternative methods (pitot tube, oil flow, orifice dam, etc.), the hot-wire gage has a very small effective dimension and, because of its small size, it can be calibrated without considering the type of boundary-layer flow.[3] Moreover, the hot-wire gage does not suffer from the shortcomings of the classic pressure probe methods such as low spatial resolution, slow response, and possible disturbance to the sensitive flowfield. Its principle of operation is based on measurement of the temperature differences between two sensors located on both sides of a buried heat source. The heat convected locally from the heat source to the sensor downstream causes the downstream sensor to sense higher temperatures than the upstream sensor. When the gage is in a separation region where the flow direction is reversed, heat is convected upstream (relative to the main flow) and the sign of the temperature difference between the two sensors is changed.

A numerical analysis of the conjugated problem of a supersonic boundary-layer flowfield (turbulent and laminar) and a conductive solid wall has been made recently[4,10] to simulate a two-dimensional gage. The results were discussed with emphasis on the effect of the various parameters in determining the sensitivity of the gage and on the influence of the gage on the flowfield. These results indicated that even in the case of high heat source intensity, the influence of the gage on boundary-layer flows was minimal. The question of the sensitivity of such a gage and its influence on the flowfield in the vicinity of a separation bubble is considered here.

As a test case, the supersonic turbulent flow over a compression corner[5] was selected. This case has been investigated extensively, experimentally as well as numerically, and the small separation bubble (which was confined to the ramp-plate juncture), allowed the use of a very fine computational grid in this region.

The gage performance is modeled in the present paper by a solution of the two-dimensional, time-dependent Navier-Stokes equations for compressible turbulent flow coupled with a solution of the heat conduction equation for the solid wall where the gage is simulated by a line heat source embedded in the wall.

Although a thin-layer approximation[6] for solving certain flowfields is often sufficient,[7,8] it was criticized recently as being invalid at separation and inadequate for unsteady (transonic) flows.[9] For these reasons, a full Navier-Stokes implicit algorithm is used here. (No evidence was found from any calculation of a significant discrepancy between the thin-layer approximation and the Navier-Stokes equations.[8]) A very fine grid is used in the vicinity of separation bubble in order to resolve small changes in the flowfield. The results are discussed, with emphasis on the effect of the heat source location and its strength on the bubble for both a steady heat

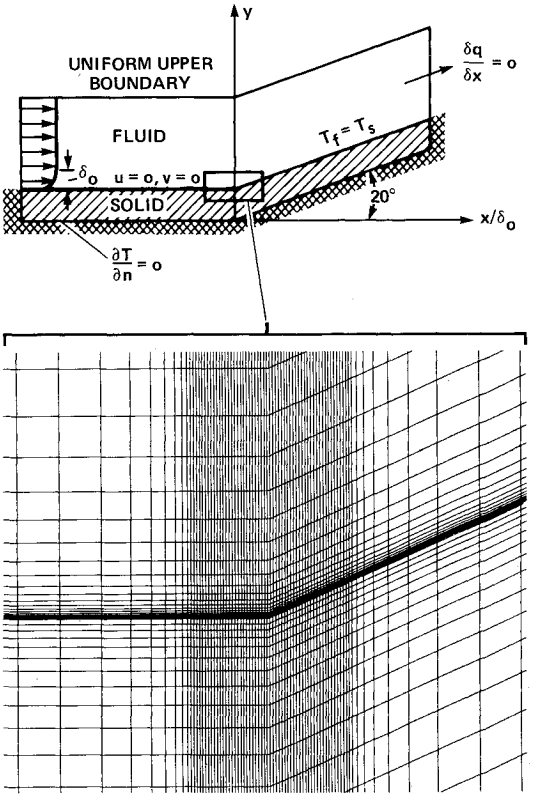

Fig. 1 Computational domain.

Received Oct. 19, 1982; revision received Jan. 30, 1984. This paper is declared a work of the U.S. Government and therefore is in the public domain.

*NRC Senior Research Associate (on leave from Faculty of Mechanical Engineering, Technion—Israel Institute of Technology, Haifa, Israel). Member AIAA.

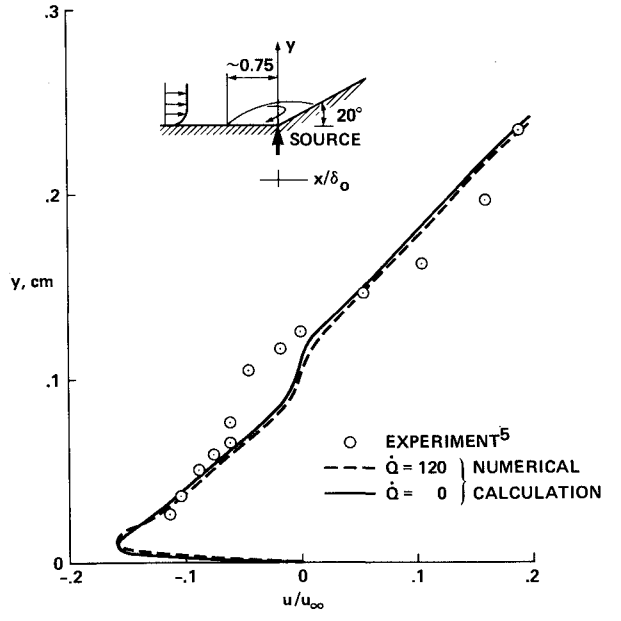

Fig. 2 Comparison of velocity profiles computed and measured at $x=0$.

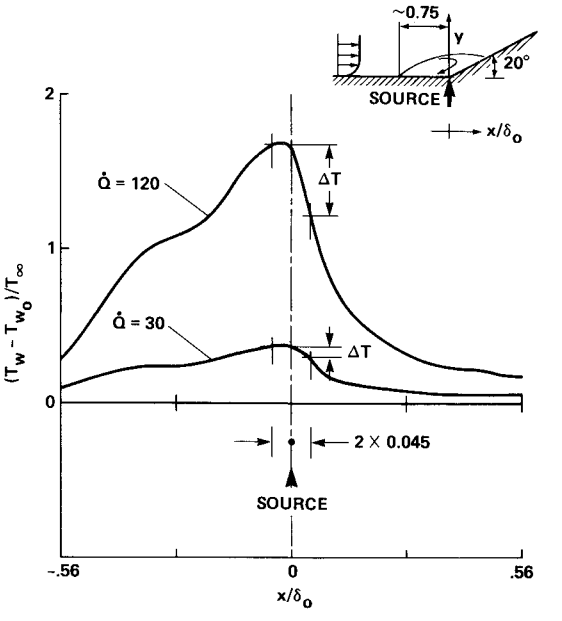

Fig. 3 Computation of surface temperature for various heat sources located at $x=0$.

source and a temperature pulse and on the corresponding performance of the separation gage.

Governing Equations

Flowfield

The strong conservation law form of the Navier-Stokes equations in general coordinates can be written in non-dimensional form[8,11] as

$$\frac{\partial \hat{q}}{\partial \tau}+\frac{\partial \hat{E}}{\partial \xi}+\frac{\partial \hat{F}}{\partial \eta}=Re^{-1}\left[\frac{\partial}{\partial \xi}(\hat{R}^{\xi}+\hat{R}^{\eta})+\frac{\partial}{\partial \eta}+(\hat{S}^{\xi}+\hat{S}^{\eta})\right] \quad (1)$$

The inviscid flux vectors in Eq. (1) are

$$\hat{q}=\bar{q}/J$$

$$\hat{E}=(\xi_t\bar{q}+\xi_x\bar{E}+\xi_y\bar{F})/J$$

$$\hat{F}=(\eta_t\bar{q}+\eta_x\bar{E}+\eta_y\bar{F})/J \quad (2)$$

and the viscous flux vectors are

$$\hat{R}=\hat{R}^{\xi}(\bar{q},\bar{q}_{\xi})+\hat{R}^{\eta}(\bar{q},\bar{q}_{\eta})=(\xi_x\bar{R}+\xi_y\bar{S})/J$$

$$\hat{S}=\hat{S}^{\xi}(\bar{q},\bar{q}_{\xi})+\hat{S}^{\eta}(\bar{q},\bar{q}_{\eta})=(\eta_x\bar{R}+\eta_y\bar{S})/J \quad (3)$$

where $\bar{E}$, $\bar{F}$, $\bar{R}$, and $\bar{S}$ are the flux vectors in Cartesian coordinates and J the transformation Jacobian.

Sutherland's law is used to calculate the laminar viscosity. The effects of turbulence are simulated in terms of an eddy viscosity coefficient, using the algebraic model of Baldwin and Lomax.[7]

Solid Wall

The two-dimensional, time-dependent heat conduction equation for general coordinates in nondimensional form is[11]

$$T_{\tau}=\bar{\alpha}\{J^2[A_1T_{\xi\xi}+A_2T_{\eta\eta}-2A_3T_{\xi\eta}]$$

$$+J^3[T_{\xi}(A_4x_{\eta}-A_5y_{\eta})+T_{\eta}(A_5y_{\xi}-A_4x_{\xi})]\}+\delta\dot{Q} \quad (4)$$

where T is the solid temperature, $\bar{\alpha}$ the thermal diffusivity, and $\delta=\delta(x,y)$ the location of the heat source $\dot{Q}$, $\dot{Q}=\dot{q}L/T_{\infty}a_{\infty}\rho_s c_s$.

The wall exchanges heat with the fluid through the fluid/solid interface only and is insulated on the other three sides. To satisfy the temperature and heat flux continuity requirements, the interface matching conditions are

$$T_{\text{fluid}}=T_{\text{solid}}$$

$$k_s(T_{\eta})_{\text{solid}}=k_f(T_{\eta})_{\text{fluid}} \quad (5)$$

where k_s and k_f are the solid and the fluid conductivities.

Equations (1) and (4), with the proper boundary conditions, are solved simultaneously using implicit algorithms.[11] The numerical technique and the treatment of boundary and initial conditions are given in Refs. 6 and 11.

Results

The computational domain and the appropriate boundary condition are shown in Fig. 1. A stretched grid in the normal direction is used near the wall for resolving the viscous layer. Also, a fine grid is used along the bubble and is stretched to a coarser grid outside the bubble ($\Delta x/\delta_0=0.045$ in the bubble, where δ_0 is the boundary-layer thickness upstream of the bubble and $\Delta x/\delta_0=0.64$ outside the bubble). A total of 120×48 points is used in the fluid region. In the solid region, 120×30 points are used with the same spacing in the x direction as in the fluid region. On a CDC 7600 computer, 2.2 s per time step is required for this grid.

The code was run first for steady-state cases for different corner angles of 15-24 deg and the computed results agree with other calculations.[5,7]

Effect of Heat Source: Steady State

In these cases, a line heat source was "buried" close to the wall surface. The nondimensional conductivity for the substrate material of the wall was chosen to be $k^*=k_s/k_{\infty}=5.85$, as was used by Mateer et al. in their experiments.[2] The calculations started with the steady-state solution of a 20 deg compression corner as the initial data, the heat source was turned on, and a new steady state was computed (starting from a steady-state solution of a 20 deg

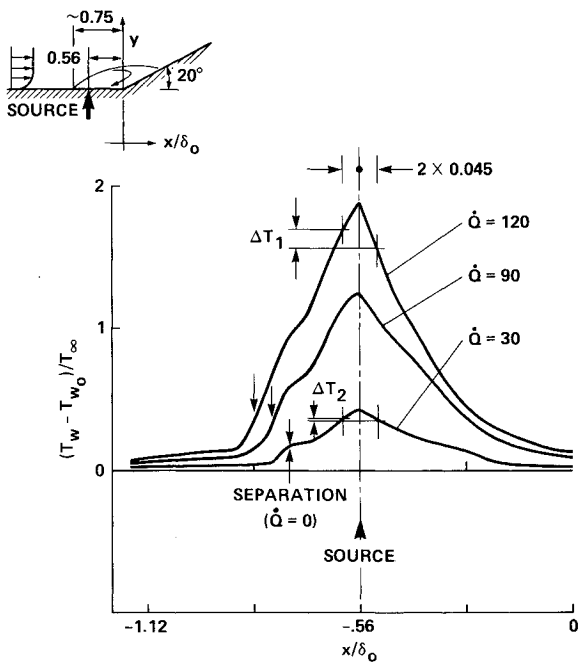

Fig. 4 Computation of surface temperature for various heat sources located at $x = -0.56\,\delta_0$.

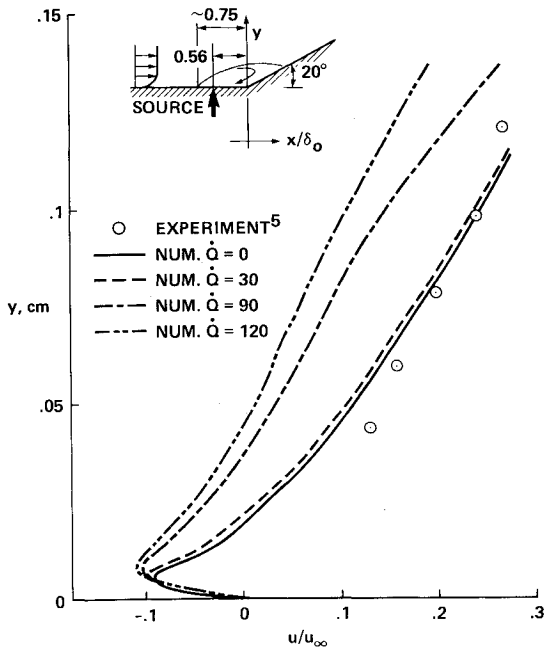

Fig. 5 Comparison of velocity profiles computed and measured at $x = -0.56\,\delta_0$.

compression corner as the initial data, the program requires about 600 steps to reach a new steady state with the heat source turned on).

The determine the effect on the flowfield of the heat released by the gage, it was first located on the plate-ramp juncture (Figs. 2 and 3). Figure 2 shows the computed u/u_∞ velocity component plotted against the distance above the wall for nondimensional source strengths of $\dot{Q}=0$ and $\dot{Q}=120$ along with experimental data.[5] The heat source has very little effect on the flowfield, even for this high heat source strength ($\dot{Q}=120$). However, by plotting the surface temperature for various heat sources (Fig. 3), one can see the large temperature differences obtained even for a relatively low heat source strength ($\dot{Q}=30$).

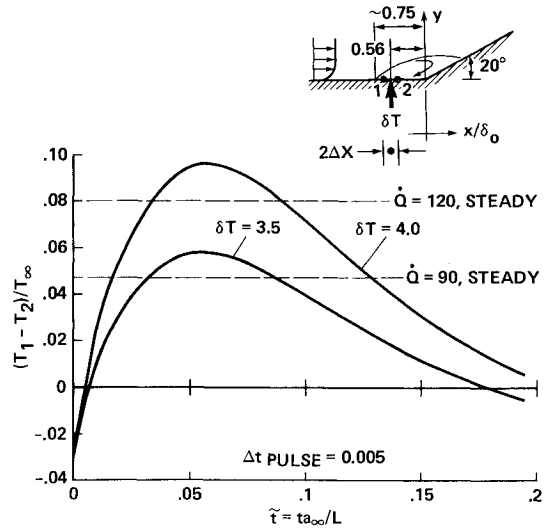

Fig. 6 Changes of $T_1 - T_2$ with time after a temperature pulse at $x = -0.56\,\delta_0$

The basic concept of the separation gage is that the temperature differences in the wall upstream and downstream of the heat source change sign when the flow separates in the vicinity of the gage. Following this idea, the heat source was next located close to the separation ($0.186\,\delta_0$ from the separation point or $x = -0.56\,\delta_0$).

Figure 4 shows the surface temperature distribution for different heat source strengths. Here, for $\dot{Q}=120$, only a small temperature difference (ΔT_1) is seen when "sensors" are placed $\pm 0.045\,\delta_0$ upstream and downstream of the heat source. For $\dot{Q}=90$ the temperature difference is smaller and for $\dot{Q}=30$ it has almost vanished (ΔT_2). The arrows on the left side of Fig. 4 show the location of the flow separation point for each source strength. Figure 5 shows the effect of these heat sources on the flowfield. It is clear that to obtain significant temperature differences (i.e., $\dot{Q}>30$), the flowfield is highly distorted by the heat source in the vicinity of separation. However, it was also found (but not shown here) that by decreasing the wall conductivity or by placing the source closer to the fluid/solid interface, one can increase the detected temperature differences.

Effect of Heat Source: Temperature Pulse

Here again the steady-state solution of the flow over a 20 deg compression corner was used as initial data. At time = 0, an intense pulse δT was imposed at the fluid/solid interface (at $X_{\text{pulse}} = -0.56\,\delta_0$) for a short period of time δ_t and then the transients of the flowfield and solid temperature field were calculated.

Figure 6 presents the change with time of the temperature difference between two grid points, $T_1 - T_2$, located at $X_{\text{pulse}} \pm 0.045\,\delta_0$ (see upper right corner of Fig. 6). Two cases are presented ($\delta T = 3.5$ and 4.0) along with the constant values representing $T_1 - T_2$ of the steady heat source cases from Fig. 4. At time = 0, $T_1 - T_2$ is negative, but after a very short time $T_1 - T_2$ becomes positive (i.e., the convection of the pulse toward point 1 in the separated flow causes a higher temperature at that point relative to point 2). The difference $T_1 - T_2$ reaches a peak and dies away as the heat dissipates in the flowfield by convection and conduction. Note that the maximum values of $T_1 - T_2$ for these cases are larger than those of the steady-state case $\dot{Q}=90$ and are almost as large as the one of $\dot{Q}=120$.

To determine the effect of these pulses on the flowfield, the changes with the time of skin friction at the pulse location $x = -0.56\,\delta_0$ are plotted in Fig. 7, along with values from the

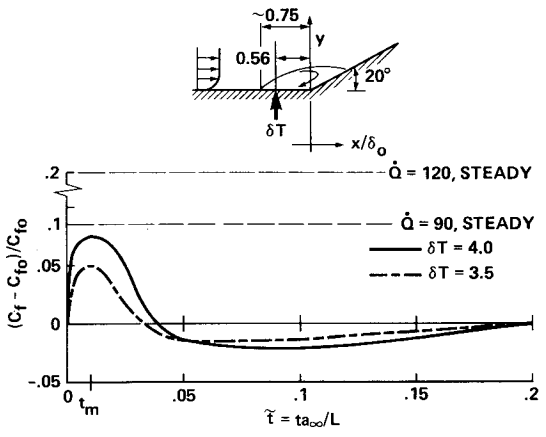

Fig. 7 Effect of temperature pulse at $x = -0.56\ \delta_0$ on skin friction.

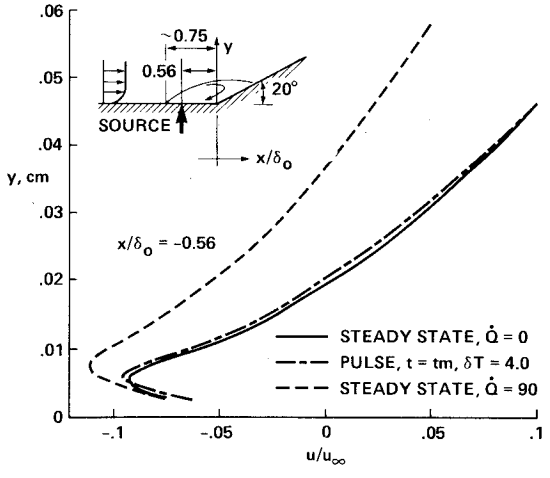

Fig. 8 Computed velocity profiles at $x = -0.56\ \delta_0$.

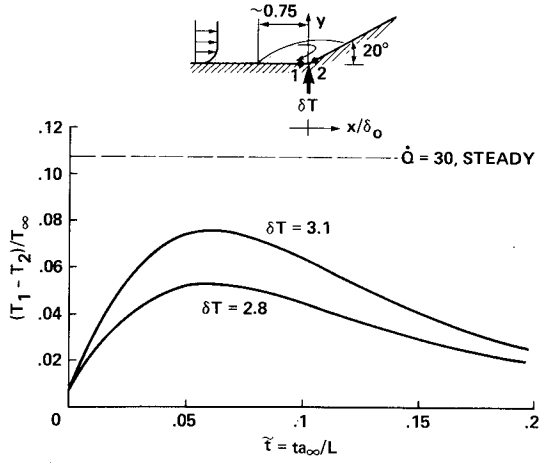

Fig. 9 Changes of $T_1 - T_2$ with time after a temperature pulse at $x = 0$.

steady heat source cases. It is clear from Figs. 6 and 7 that the temperature pulse causes less distortion to the flowfield than the steady heat source for comparable flow detection sensitivity. Also, one can see that nearly maximum $T_1 - T_2$ is reached when the change in the skin friction is very small (at time = 0.05).

Figure 8 presents the velocity profiles at $x = -0.56\ \delta_0$. The velocity profile of the pulse case is plotted at $t = t_m = 0.01$ where ΔC_f reaches its maximum (Fig. 7). One can see from Fig. 8 how small the effect of the pulse is relative to the steady-state heat source cases, even at its maximum disturbance.

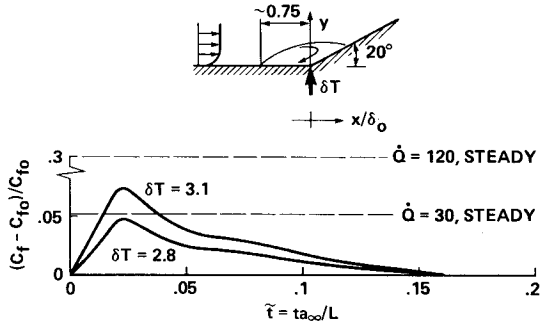

Fig. 10 Effect of temperature pulse at $x = 0$ on skin friction.

Figures 9 and 10 present similar pulsed cases with the source placed at $x = 0$. Although the pulse method with $\delta T = 2.8$ or 3.1 shows the direction of the flow almost as well as the steady $\dot{Q} = 30$ case, as one can see from Fig. 9, higher flowfield distortion (i.e., changes of skin friction, Fig. 10) occurs relative to the comparable steady-state case.

Conclusions

By using the numerical simulation of the conjugated solid-supersonic flowfield problem, the effect on the flow of a line heat source located on the solid surface within a separation bubble was studied. For steady heat source cases, it was found that, if a heat source is located near the separation point and is of low enough strength not to distort the flowfield, the flow direction near the wall can barely be detected with upstream and downstream surface temperature detectors. When the heat source is located on the wall well inside the separation bubble, the convection from the heat source easily shows the direction of the flow.

The difference between the two cases of the heat source location can be explained by the fact that, near the separation point, the bubble is extremely thin and the convection of heat in the bubble is lower compared with the heat conduction in the wall. This situation can be improved by decreasing the wall conductivity or by placing the source closer to the solid/fluid interface. This explanation may clarify why the pulse gives better results than the steady heat source near separation. Since the time needed for high-temperature pulses to dissipate by convection is much shorter than the corresponding conduction time, the temperature changes near the wall respond chiefly to the convection of the pulse heat. The fast dissipation of the pulse and the relaxation of the flowfield may suggest a possible way of scanning many points along the wall in a very short time. Two wires on either side of a third wire (the heat source) may be used as sensors. By embedding a large number of wires in the wall, one may use the wires alternately, three at a time, down the wall as sensors and heat sources.

The author must emphasize that, although the code and the technique discussed in this paper were checked very carefully and the numerical results agree very well with steady-state experimental cases, the pulse technique suggested here has never been tested experimentally. Moreover, most of the experimental gages have three-dimensional effects (i.e., a short, heated element embedded under almost a two-dimensional type of flow). In the present simulation, the heat source is purely two-dimensional (mainly because of computer power limitations) and thus has a larger effect on the flowfield.

References

[1] Higuchi, H. and Peake, D. J., "Bi-Directional Buried Wire Skin Friction Gage," NASA TM-78531, 1978.

[2]Mateer, G. G., Brosh, A., and Viegas, J. R., "A Normal Shock-Wave Turbulent Boundary Layer Interaction at Transonic Speed," AIAA Paper 76-161, 1976.

[3]Rubesin, M. W., Okuno, A. T., Mateer, G. G., and Brosh, A., "A Hot Wire Surface Gage for Skin Friction Measurements and Separation Detection," NASA TMX 62-465, 1975.

[4]Degani, D., Brosh, A., and Shemesh, L., "Buried Wire Separation Detector Simulation in Compressible Flow," *AIAA Journal*, Vol. 19, July 1981, pp. 952-954.

[5]Horstman, C. C., Hung, C. M., Settles, G. S., Vas, I. E., and Bogdonoff, S. M., "Reynolds Number Effects on Shock-Wave Turbulent Boundary Layer Interaction—A Comparison of Numerical and Experimental Results," AIAA Paper 77-42, 1977.

[6]Steger, J. L., "Implicit Finite Difference Simulation of Flow about Arbitrary Two-Dimensional Geometries," *AIAA Journal*, Vol. 16, July 1978, pp. 679-686.

[7]Baldwin, B. S. and Lomax, H., "Thin Layer Approximation and Algebraic Model for Separated Turbulent Flows," AIAA Paper 78-257, 1978.

[8]Degani, D. and Steger, J. L., "Comparison Between Navier-Stokes and Thin Layer Computation for Separated Supersonic Flow," *AIAA Journal*, Vol. 21, Nov. 1983, pp. 1604-1607.

[9]Chyu, W. J. and Kuwahara, K., "Computations of Transonic Flow over an Oscillating Airfoil with Shock-Induced Separation," AIAA Paper 82-350, 1982.

[10]Degani, D. and Brosh, A., "Numerical Simulation of a Compressible Turbulent Boundary Layer Over a Conductive Wall with Line Heat Source," *Computers and Fluids*, Vol. 11, 1983, pp. 85-93.

[11]Degani, D., "Numerical Study of the Effect of an Embedded Surface-Heat Source on the Separation Bubble of Supersonic Flow," AIAA Paper 83-1753, 1983.